Article

Microscopic Origin of Magnetization Reversal in Nanoscale Exchange-Coupled Ferri/Ferromagnetic Bilayers: Implications for High Energy Density Permanent Magnets and Spintronic Devices

Michael Heigl,* Christoph Vogler, Andrada-Oana Mandru, Xue Zhao, Hans Josef Hug, Dieter Suess, and Manfred Albrecht

Read Online

ACCESS | Metrics & More | Article Recommendations

ABSTRACT: Giant exchange bias shifts of several Tesla have been reported in ferrimagnetic/ferromagnetic bilayer systems, which could be highly beneficial for contemporary high energy density permanent magnets and spintronic devices. However, the lack of microscopic studies of the reversal owing to the difficulty of measuring few nanometer-wide magnetic structures in high fields precludes the assessment of the lateral size of the inhomogeneity in relation to the intended application. In this study, the magnetic reversal process of nanoscale exchange-coupled bilayer systems, consisting of a ferrimagnetic TbFeCo alloy layer and a ferromagnetic $[Co/Ni/Pt]_N$ multilayer, was investigated. In particular, minor loop measurements, probing solely on the reversal characteristics of the softer ferromagnetic layer, reveal two distinct reversal mechanisms, which depend critically on the thickness of the ferromagnetic layer. For thick layers, irreversible switching of the macroscopic minor loop is observed. The underlying microscopic origin of this reversal process was studied in detail by high-resolution magnetic force microscopy, showing that the reversal is triggered by in-plane domain walls propagating through the ferromagnetic layer. In contrast, thin ferromagnetic layers show a hysteresis-free reversal, which is nucleation-dominated due to grain-to-grain variations in magnetic anisotropy of the Co/Ni/Pt multilayer and an inhomogeneous exchange coupling with the magnetically hard TbFeCo layer, as confirmed by micromagnetic simulations.

KEYWORDS: *TbFeCo, ferrimagnet, magnetization reversal, exchange spring systems, MFM, micromagnetic, modeling, spintronics, high energy density permanent magnets*
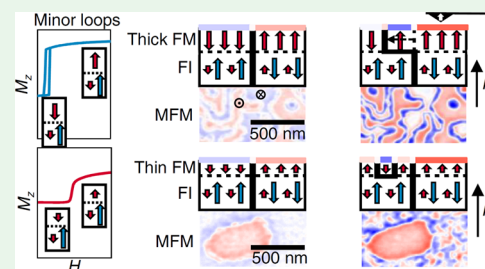
INTRODUCTION

The concept of engineering exchange-coupled composites is the most promising approach to meet current challenges in fabricating high energy density permanent magnets.[1−3] Already in 1991, Kneller and Hawig[4] proposed to manufacture magnets with a magnetically hard and soft phase, exchange-coupled at a mutual interface. While the high magnetocrystalline anisotropy of the hard phase provides a high coercive field, the coupled soft phase should contribute to the energy density product by a high saturation magnetization. Due to the soft phase, the demagnetization curve shows a completely reversible part, which led to the term "exchange-spring magnets". Furthermore, exchange-coupled systems employing ferrimagnetic (FI) heavy rare earth (RE)-3d transition metal (TM) alloys provide high tunability, interfacial exchange interaction, and zero magnetic moment at the compensation temperature T_{comp},[5−17] which is highly beneficial for many applications such as spin valves[18−23] and magnetic tunnel junction devices.[24] Below T_{comp}, the magnetic moment of the RE atoms dominates, which leads to an antiparallel alignment of the net magnetic moments of the FI layer when coupled to a ferromagnetic (FM) layer. As a consequence, a positive horizontal shift of the hysteresis loop of the magnetically softer layer is typically observed after saturation in the positive field direction. In this configuration, a giant exchange bias shift of several Tesla has been reported for various nanoscale FI/FM bilayer systems that can differ in the reversal behavior of the soft layer exhibiting either fully reversible or irreversible switching.[11,25−28]

Micromagnetic simulations showed that a partial domain wall is formed at the FI/FM interface layer during the reversal of the FM.[29] The minor loop becomes fully reversible if this domain wall generates a hard-axis field that overcomes the anisotropy field of the FM. It was further reported that the anisotropy and the bulk exchange of both layers as well as the exchange coupling strength and the thickness of the FM play an important role in
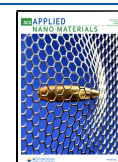
the reversibility of the FM. The underlying reversal mechanism for reversible switching was studied in detail in a $[Co(0.4 \text{ nm})/Pt(0.7 \text{ nm})]_5$ multilayer exchange-coupled to ferrimagnetic $Tb_{26.5}Fe_{73.5}$ (20 nm), which acts as a magnetically hard pinning layer. There, a nucleation-dominated magnetization reversal process was revealed, which is caused by grain-to-grain variations in magnetic anisotropy of the Co/Pt multilayer (ML) and an inhomogeneous exchange coupling to the magnetically hard TbFe layer.[30]

In a recent study on a nanometer-thick $TbFeCo/[Co/Ni/Pt]_N$ sample series, we have systematically investigated the reversal behavior of the softer FM layer as a function of its thickness, including a detailed theoretical analysis of the full reversibility condition.[29] In the present work, we study in detail two specific FI/FM samples out of this sample series exhibiting two distinct cases of reversible and irreversible switching. The different underlying microscopic reversal processes are investigated using high-resolution magnetic force microscopy and micromagnetic simulations. Having a detailed understanding of such complex magnetization reversals is crucial for future spintronic and high energy density permanent magnet devices.

EXPERIMENTAL DETAILS

Film deposition was performed at room temperature by dc magnetron (co-)sputtering from elemental targets on a Si(001) substrate with a 100 nm-thick thermally oxidized SiO_x layer. The sputter process was carried out using an Ar working pressure of 5×10^{-3} mbar in an ultrahigh vacuum chamber (base pressure $< 10^{-8}$ mbar). The heterostructures consist of a 20 nm-thick amorphous ferrimagnetic $Tb_{28}Fe_{58}Co_{14}$ layer[17] and a ferromagnetic $[Co(0.2 \text{ nm})/Ni(0.4 \text{ nm})/Pt(0.6 \text{ nm})]_N$ ML on top (Figure 1). In addition, a 5 nm-thick Pt seed
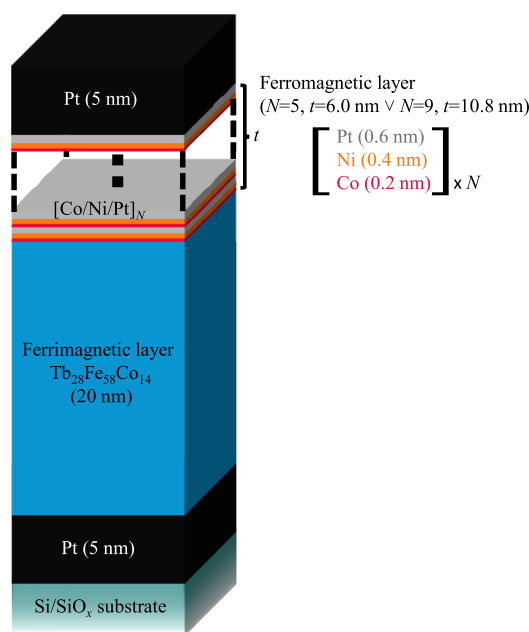

Figure 1. Schematic image illustrating the layer stacking of the two investigated FI/FM heterostructures.

and cover layers were used. The thicknesses of the layers were estimated from the areal densities measured by a quartz balance during deposition, while the elemental composition of the TbFeCo alloy as well as the calibration of the quartz balance was evaluated by Rutherford backscattering spectrometry. Two FI/FM heterostructures with different repetition numbers ($N = 5$ and 9) of the ferromagnetic multilayer were chosen for this study, exhibiting different reversal

mechanisms.[29] Furthermore, reference samples of the individual layers were prepared.

The integral magnetic properties of the FI/FM heterostructures were investigated by superconducting quantum interference device—vibrating sample magnetometry (SQUID-VSM). All $M-H$ minor and full loops were measured at 40 K in the out-of-plane geometry, revealing for both systems strong perpendicular magnetic anisotropy where the ferrimagnetic layer acts as a magnetically hard pinning layer. Furthermore, the ferrimagnet is Tb-dominant over the entire temperature range that we investigated, meaning that the Tb magnetic moment is always larger than the total Co/Ni moment. Consequently, the net moments of the FI/FM heterostructures are antiferromagnetically aligned in the ground state at zero field. The magnetic properties of the full sample series can be found in ref 29. More details on the magnetic properties of Co/Ni/Pt MLs can be found in ref 31.

Complementary, the complex reversal behavior was locally imaged at 40 K by an ultrahigh vacuum magnetic force microscope operating in magnetic fields of up to 7 T.[32] Details on the magnetic force microscopy (MFM) data acquisition and data processing can be found in refs 30 and 33.

EXPERIMENTAL RESULTS

Macroscopic Minor Loop Studies. The $M-H$ full hysteresis and also minor loops of the exchange-coupled FI/FM systems and of reference samples consisting only of the FI or FM layers recorded at 40 K are shown in Figure 2. Both reference samples show strong
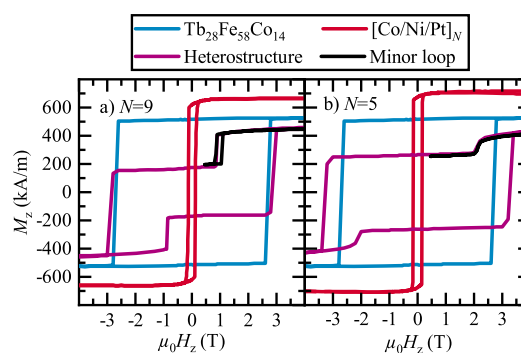

Figure 2. $M-H$ hysteresis loops of the FI/FM heterostructures obtained at 40 K. (a) Thicker FM layer ($N = 9$) switches irreversibly as apparent from the presence of a hysteresis in the minor loop (black). (b) In contrast, the thinner FM layer ($N = 5$) exhibits a fully reversible switching, as shown by the minor loop (black). The $M-H$ hysteresis loops of the individual layers forming the heterostructures are displayed as well.

perpendicular magnetic anisotropy with coercive fields of about 3 T for the FI layer and 200 mT for the Co/Ni/Pt MLs. For the exchanged-coupled FI/FM heterostructures, starting from saturation, by lowering the magnetic field, the FM layer reverses due to the strong antiferromagnetic coupling. At a high opposite field of about 3 T, eventually, the magnetically hard FI layer switches. It is observed that the field required for reversing the FM layer becomes larger with decreasing number N (thickness), which is expected if the interfacial exchange coupling remains constant.[29,34] The minor loops were captured to analyze the switching process of the softer FM layer and show two distinct switching mechanisms. While the FI/FM heterostructure with the thick FM layer exhibits a hysteretic reversal process (Figure 2a), the thinner FM layer reveals fully reversible switching (Figure 2b).

High-Resolution Magnetic Force Microscopy Studies. Here, we concentrate on studying the thicker FM layers ($N = 9$) to extract the microscopic mechanisms leading to the transition from a nonhysteretic to hysteretic minor loop magnetization process when increasing the FM layer thickness from $N = 5$ to 9. For this, the sample was demagnetized to acquire the virgin $M-H$ dependence at 40 K for fields raised from 0
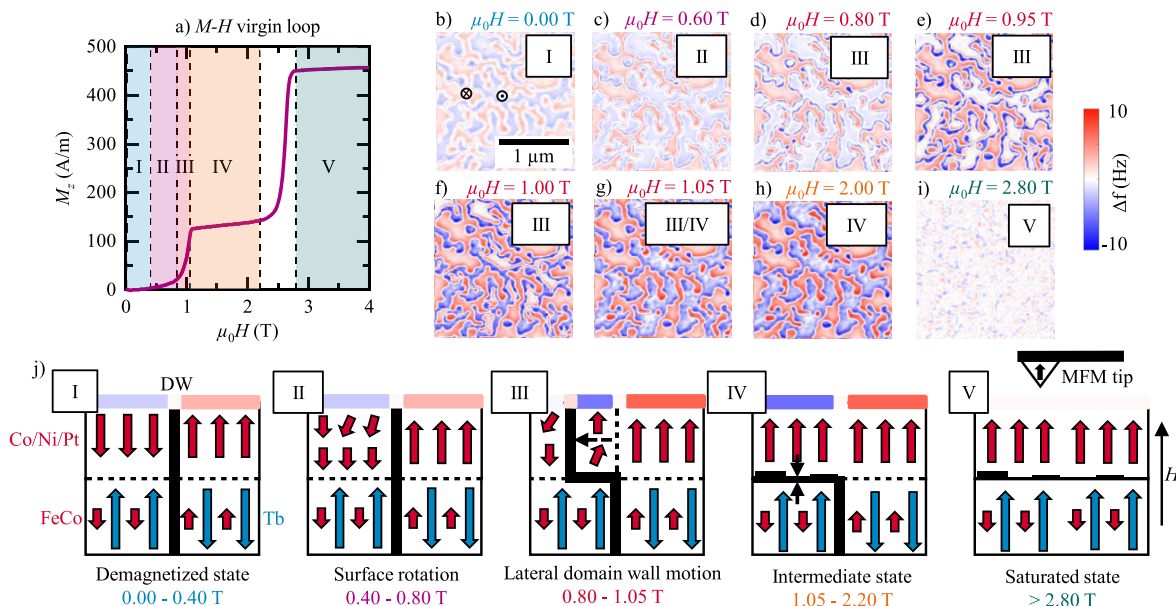
Figure 3. (a) Virgin $M-H$ curve of the FI/FM heterostructure with $N = 9$ taken at 40 K starting from the demagnetized state. Five distinct field ranges are highlighted by different background colors. (b–i) In-field MFM images ($2\,\mu m \times 2\,\mu m$) are displayed with an applied magnetic field ranging from 0 up to 2.80 T. (j) Schematics of the magnetic states typical for the five field ranges.
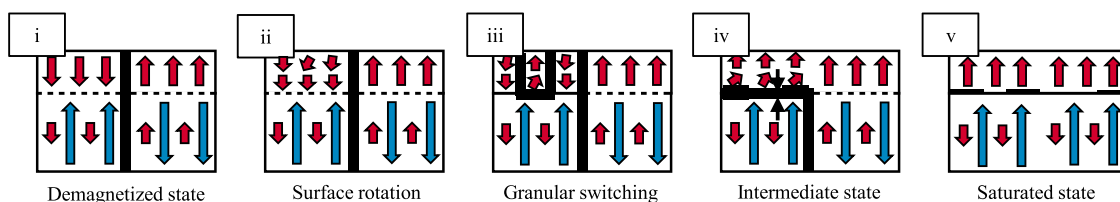

Figure 4. Schematic showing the underlying microscopic reversal mechanism for fully reversible switching via granular nucleation.[30]

to 4 T (Figure 3a). A different piece of the same sample in its as-grown state was used to acquire a series of MFM images at 40 K in fields from 0 to 2.8 T (Figure 3b−i). The magnetic domain structure in the as-grown state is presented in Figure 3b. In this state, the net magnetic moment of the FI layer and the magnetic moment of the FM layer are aligned antiparallel, which is the ground state of this exchange-coupled FI/FM system. Because the tip magnetization is along the positive field direction (up), the domains appearing with a negative frequency shift contrast (blue domains) have a net up magnetization (parallel to that of the tip), while the red domains have a net down magnetization. The domains are separated by vertical domain walls going through both layers, as schematically displayed in Figure 3j-I. The magnetization loops acquired for the FI/FM heterostructure sample (the purple loop in Figure 2a and the virgin loop displayed in Figure 3a) reveal that the Tb magnetic moment dominates the Co and Fe moments of the FI layer and also those of the FM layer. Hence, the blue domains are locations characterized by an up magnetization of the FI layer and a down magnetization of the FM layer. When the field is increased to 0.6 T (Figure 3c), a slight increase of the MFM contrast is observed that is compatible with a small rotation of the magnetic moments at the top of the FM layer away from the initial down direction toward the up direction schematically shown in Figure 3j-II. A more noticeable change becomes apparent at 0.8 T (Figure 3d): here, some dark blue spots occur at the domain walls and the overall contrast is further increased. The latter is compatible with an increase of the rotation of the magnetic moments at the top of the FM layer. The dark blue spots near the domain walls indicate the beginning of a lateral domain wall motion (Figure 3j-III) that becomes clearly visible in Figure 3e,f for fields of 0.95 and 1 T, respectively. At about 1.05 T (Figure 3g), the FM layer is almost fully reversed. The remaining MFM contrast then predominantly arises from the domains of the FI layer. For fields between 1.05 and 2 T, the MFM contrast increases only very slightly, which is

compatible with a vertical compression of the horizontal domain wall that has formed at the locations of the blue domains at the FI/FM interface (Figure 3j-IV). Note however that no further lateral domain wall motion occurs. This reflects the high coercivity of the FI layer. The last MFM image (Figure 3i) shows a state where all down domains in the FM have been erased, and an in-plane interfacial domain wall has formed (Figure 3j-V).[26] The weak granular contrast is caused by variations of the z component of the magnetic moment density arising, for example, from spatial film inhomogeneities (e.g., in the TbFeCo composition[35,36]).

The details of the underlying reversal mechanism of the fully reversible switching case were already reported for a similar TbFe/[Co/Pt]₅ heterostructure.[30] There, a nucleation-dominated three-stage magnetization reversal process was revealed, which is caused by grain-to-grain variations in magnetic anisotropy of the Co/Pt ML and an inhomogeneous exchange coupling to the magnetically hard TbFe layer. The reversal steps are schematically illustrated in Figure 4. They consist of a rotation-dominated part of the FM layer starting at the top surface of individual grains (ii) followed by the full reversal (iii) till saturation (iv). The last reversal step is again characterized by a rotation part of the FI domains till saturation (v).

■ MICROMAGNETIC SIMULATIONS

In this section, finite element simulation results obtained with the finite element package magnum.fe[37] are presented. This is to reproduce the different minor loop behaviors observed for thin and thick FM layers and from that gain a more fundamental understanding of the relevant physics governing the experimental observations.

As shown in Figure 5, we model 100 nm × 100 nm films consisting of a 20 nm-thick FI layer and FM layers of a 6.0 and
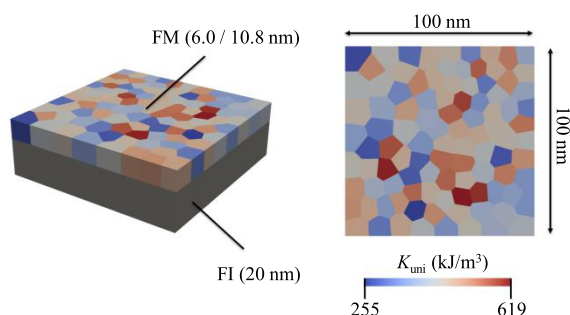

Figure 5. Model of the simulated FI/FM bilayer structure. The lateral dimension of the model and the thickness of the layers are given. The average grain diameter is 10 nm, and the discretization length is 2 nm. The color code shows the effective magnetic anisotropy, which is assumed to be normally distributed over the grains in the FM layer.

10.8 nm thickness, corresponding to the two different repetition numbers of $N = 5$ and 9, respectively. The structures consist of grains having an average diameter of 10 nm, generated by Voronoi tessellation. Due to the required small discretization length of 2 nm and the resulting large computational effort, the lateral dimensions are kept at 100 nm × 100 nm, which is considerably smaller than the typical domain structures observed by MFM, as displayed in Figure 3b−i. However, given that single grains with a lateral length of 50 nm were well approximated with a spin chain model in a previous work,[30] a homogeneous magnetization within this distance in the in-plane direction can be assumed. Hence, the lateral film dimensions for our simulation work are justified. The grains of our model are fully exchange-coupled in the lateral directions. The uniaxial magnetic anisotropy K_u is normally distributed with a mean of 430 kJ/m^3 and a standard deviation of 75 kJ/m^3 (total range of 255−619 kJ/m^3), and the ratio $J_{iex}/K_{eff,FM}$ of interface exchange constant between the two layers and the respective effective magnetic anisotropy constant of the FM is kept constant at −0.1 μm (see the color code in Figure 5). All other material parameters are given in Table 1.

The assumptions of a strong variation in the magnetic anisotropy of the FM layer and simultaneously in the interface

Table 1. Material Parameters Used for the Micromagnetic Simulations of the Investigated FI/FM Heterostructures[a]

layer	FI	FM
K_u (kJ/m^3)	1168	255−619
M_S (kA/m)	517	668
A_{ex} (pJ/m)	10.0	10.0
J_{iex} (mJ/m^2)	−0.1 to −33.8	−0.1 to −33.8
α	1.0	1.0
$\angle K_{eff} e_z$ (°)	1.0	1.0
a (nm)	100.0	100.0
t (nm)	20.0	6.0/10.8

[a]K_u is the uniaxial magnetic anisotropy constant, M_S is the saturation magnetization, A_{ex} is the exchange coupling in the bulk, J_{iex} is the interface exchange coupling between the antiferromagnetically coupled layers, α is the damping constant, a is the lateral size of the modeled film, and t is the thickness of the layers. The anisotropy axis is tilted by 1° against the z direction in both layers to avoid metastable states.

exchange constant at the FI/FM interface are based on previous results reported in refs 29 and 30. In ref 30, a hysteresis-free minor loop was found for a similar heterostructure with a thin FM layer of 5.5 nm, and in ref 29, the relevant parameters and a condition for hysteresis-free minor loops were derived.

For the modeling, the ground state of the heterostructure with the FI layer magnetization pointing in the +z direction and that of the FM layer pointing in the −z direction is considered. Subsequently, the field magnitude is increased stepwise in 50 mT increments up to 4 T and then decreased back to 0 T. After each field step, the micromagnetic state of the system is relaxed for 1 ns. Note that the variation of the applied field in the simulations is performed much faster than that used during the experiments. However, because of the high damping constant (α = 1.0) used for the simulations, a stationary state is obtained within 1 ns such that the modeled loops are representative of the experimental loops.

Figure 6 displays minor loops of heterostructures with a thick ($N = 9$) and thin ($N = 5$) FM layer. While the loop for the thick
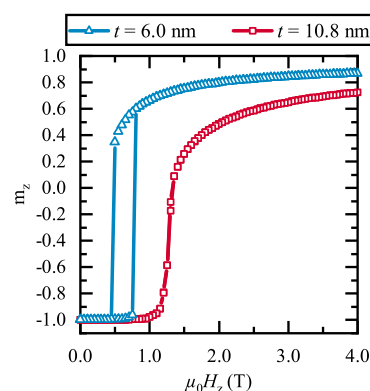

Figure 6. Simulated macroscopic minor loops of the FM layer coupled to the FI for two different FM thicknesses of 6 ($N = 5$, blue line and triangles) and 10.8 nm ($N = 9$, red lines and squares).

FM layer shows a lower switching field of about 580 mT and a hysteresis width around 300 mT, the switching field for the thin FM layer is higher than 1 T and the hysteresis is absent. This reproduces the experimentally observed switching behavior of the FM layer (see black lines in Figure 2a,b). Note that, for the modeling, the only parameter changed was the thickness of the FM layer.

To gain a more fundamental understanding of the reversal process of the FM layer and to understand the MFM contrast evolution with the field (Figure 3b−i), the quantity

$$m_{z,i} - \frac{1}{N}\sum_{i=1}^{N} m_{z,i} \qquad (1)$$

is plotted with $m_{z,i}$ being the z component of the normalized magnetization of node i of the finite element discretization and with the sum running over all N nodes of the surface mesh on the top of the FM. Note that, because a homogeneous magnetic moment distribution does not generate a stray field and hence has no MFM contrast, the average m_z component is subtracted in eq 1 to facilitate the comparison of the simulation results with MFM data. Figure 7 displays the computed field evolution of the contrast for the sample with a thicker FM layer ($N = 9$, 10.8 nm thick). At low positive fields, the top FM layer couples antiparallel to the bottom FI. Therefore, in Figure 7a−d, a
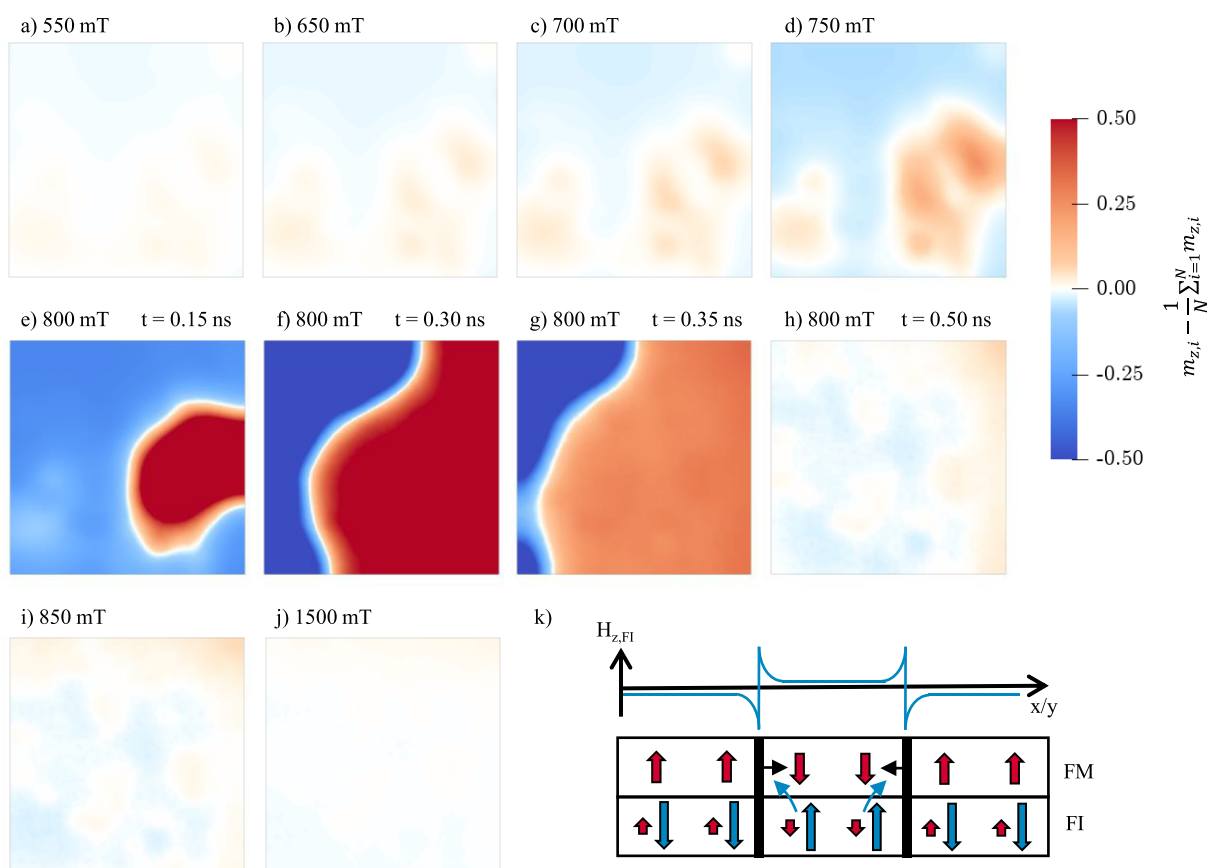
Figure 7. (a−j) Simulated MFM contrast of a thicker FM layer of 10.8 nm ($N = 9$) during its reversal for representative chosen external fields. The color code represents the quantity in eq 1. Panels (e−h) show the dynamic process of the domain wall motion during switching at 800 mT and not the relaxed magnetization state, as indicated by the simulation time. Panel (k) schematically shows the additional local field $H_{z,\mathrm{FI}}$ arising from the FI layer that hinders the lateral domain wall propagation in the FM (Figure 3d−g), in contrast to the simulation in panels (e−h).

weak contrast appears, which can be attributed to a difference in the canting of the magnetic moments in the individual grains with different magnetic anisotropy. The moments in grains with small anisotropy show more canting than those in grains with higher anisotropy. The contrast further increases with an increasing external field. Note that the simulation is performed only for the domain with an up magnetization of the FI layer and a down magnetization of the FM layer because the opposite domain with an up FM magnetization would not be affected by an applied field well below the coercivity of the FI layer. The simulation thus reveals a continuous raise of the up magnetization of the FM down domain and hence a decrease of the magnetization difference between the FM down and up domains. Therefore, the field arising from the pattern of domains in the FM that is antiparallel to that of the FI layer is reduced, and consequently, the MFM contrast is increased. This explains the small increase in contrast observed when comparing the MFM images from Figure 3b,c.

At a field of about 800 mT, a domain wall forms throughout the whole film, starting from the grain with the lowest anisotropy, as illustrated in Figure 7e−h. The domain wall propagates through the film until all parts have switched parallel to the field (and parallel to the FI net magnetization), which is a fully irreversible process in agreement with the Experimental Results. Note that, since in the relaxed magnetization state, at 800 mT, the domain wall propagation cannot be seen, Figure 7e−h shows the dynamic process at 800 mT, as indicated by the simulation time in the upper right corner. To compare the

simulation results with the observed MFM data, some limitations of the simulation work need to be further elaborated. To keep the computational effort at an acceptable level, the simulation considers only a small area within an initially down FM magnetization. Thus, the magnetostatic energy arising from the up/down FM and down/up FI domain pattern and the existence of an initial vertical domain wall inside the FI and FM is not considered. For this reason, the simulation reveals the switching of a low anisotropy grain followed by a rapid expansion of the reversal domain. In contrast, the MFM data recorded in fields from 0.8 to 1.05 T (Figure 3d−g) show steady states of the domain wall propagation that cannot be observed in the model used for simulation. The MFM images reveal that no domain reversal occurs inside the FM down domain but that the reversal starts by the propagation of an already existing wall and that the propagating wall again becomes pinned for fields from 0.8 to 1.05 T. This can be explained by the up field arising from the FI up domains, which is the strongest in the inside of the FM down domain near its wall (Figure 7k). This stray field from the FI layer adds to the applied up external field and thus drives the propagation of the existing wall to a location inside the FI up domain where the up stray field from the FI domain pattern is weaker. Because our simulation considers a FM down domain only, this behavior cannot be modeled. The simulation however reveals that, once a reversal domain exists, a rapid wall propagation follows. This explains why the field interval where a domain wall propagation is observed remains small, i.e., about
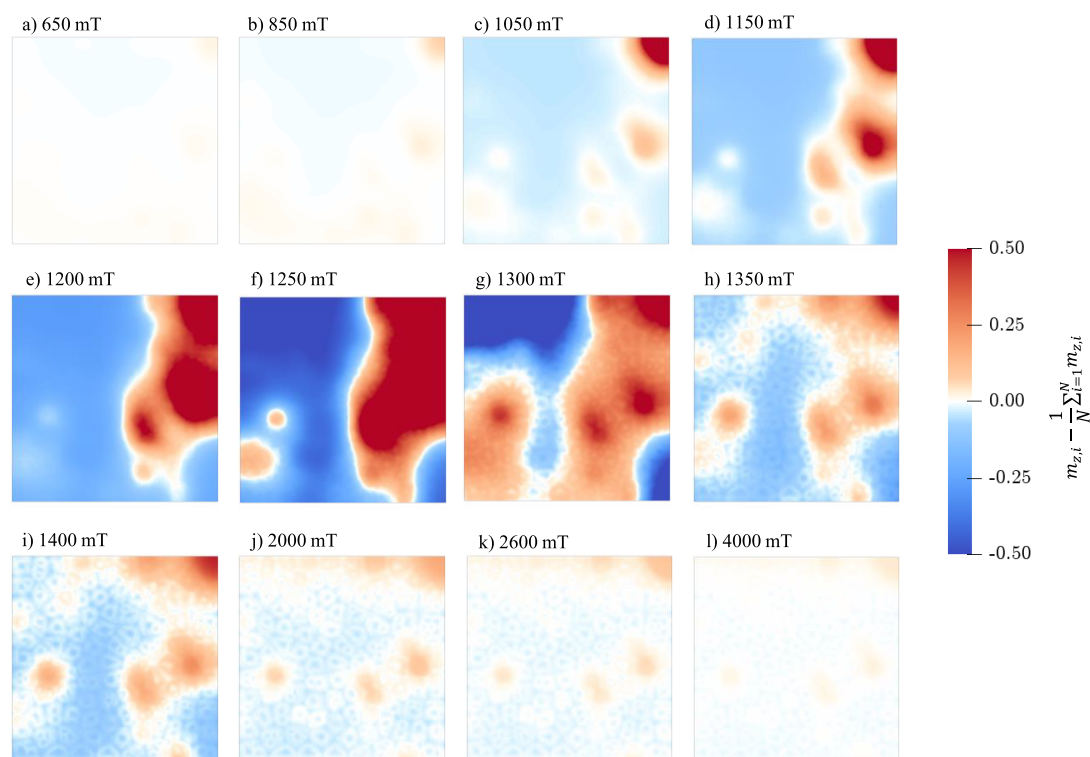
Figure 8. (a−l) Simulated MFM contrast of a thinner FM layer of 6.0 nm ($N = 5$) during its reversal for representative chosen external fields. The color code represents the quantity of eq 1.

0.2 T, which is compatible with the field on the surface of the FI layer near a domain wall.

After the FM has switched, the contrast becomes abruptly weak and decreases with increasing the external field, as displayed in Figure 7i,j. Note that, again, only the FM magnetization inside an initial FM down domain is considered. The simulation shows that the grain-to-grain variation of the up magnetic moment is reduced with increasing the up field, which corresponds to a compression of the in-plane domain wall that has formed at the FI/FM interface. Hence, the up magnetic moment of the FM layer is increased, approaching that of a FM domain with an initial up magnetization. The down/up field from the FM layer that weakened the up/down field of the domains inside the FI layer thus becomes gradually smaller. This explains the small increase of the MFM contrast observed when the field is increased from 1.05 to 2 T (Figure 3g,h).

Note that the magnetization process observed here for the thicker FM layer is fundamentally different from that observed in our previous work[30] for a thinner FM layer. For this reason, the modeling is also performed for the thinner FM layer using the parameters describing the FI/FM heterostructure samples prepared here. The results are displayed in Figure 8. Again, the modeling is performed for a film area with an initial down FM magnetization. As in our previous work,[30] a three-stage magnetization process is observed. Stage 1 (Figure 8a−c) is characterized by a rotation of the initially down magnetic moments near the top of the FM layer toward the up direction of the applied field. In stage 2 (Figure 8d−g), the magnetic moments of isolated grains switch toward the up direction to improve the alignment of the magnetic moments to the applied field. The angle between the magnetic moments and the field is then smaller for the moments near the top of the FM film and larger for those near the FI/FM interface. Because this switching

process depends on the properties of individual grains, a large grain-to-grain variation occurs. In stage 3 (Figure 8h−l), all grains have switched to have a predominately up magnetization. The contrast drops as the horizontal domain wall at the FI/FM interface is compressed, and the local variation of the domain wall thickness is decreased. As observed by MFM in our previous work,[30] no lateral propagation of a vertical domain wall inside the FM layer occurs, but a three-stage magnetization process takes place for each individual grain. This reversal process is hysteresis-free (red curve with squares in Figure 6).

The condition for hysteresis-free switching derived in ref 29 can be applied here. Using the parameters listed in Table 1 for the thicker FM layer clearly reveals that 90% of the grains in the heterostructure remain above the threshold for hysteresis-free switching ($K_{uni} \leq 330$ kJ/m^3), while for the system with the thinner FM, the threshold value is $K_{uni} \leq 418$ kJ/m^3. This means that 40% of the grains are below the threshold and hence show a hysteresis-free process. For the thinner FI/FM heterostructure with $N = 5$, this means that almost half of the FM grains show a gradual, hysteresis-free rotation of the magnetization. Based on this behavior and the small thickness of the FM, short vertical domain walls can form, as schematically illustrated in Figure 4, and the observed three-stage process with a local rearrangement of domains in the switching process occurs. In contrast, in the thick FM layer with $N = 9$, almost all grains show an irreversible, hysteretic reversal. An abrupt switch of individual grains would generate several large vertical domain walls, which is energetically unfavourable due to the thickness of the FM. This is the reason why we observe only one domain wall, which is independent from the granular structure, propagating through the FM layer and causing irreversible switching of the macroscopic minor loop.

CONCLUSIONS

We reveal two distinct magnetic reversal mechanisms in a nanometer-thick exchange-coupled bilayer system consisting of a ferrimagnetic TbFeCo alloy layer and a ferromagnetic [Co/Ni/Pt]$_N$ multilayer. The reversal characteristics depend critically on the thickness of the FM layer. By minor loop $M-H$ measurements, we observed an irreversible hysteretic switching process of the bilayer with $N = 9$ and a reversible switching for $N = 5$. The underlying microscopic origin is revealed by high-resolution MFM. For $N = 9$, the FM switches by in-plane domain wall propagation. In contrast, thinner FM layers exhibit a nucleation-dominated reversal due to grain-to-grain variations in magnetic anisotropy of the Co/Ni/Pt multilayer and an inhomogeneous exchange coupling with the magnetically hard TbFeCo layer. The coupled FM layers of both systems were modeled by finite element simulations with individual grains varying in K_u. The simulated macroscopic minor loops agreed very well with the experiments. The simulated MFM contrast of the thicker FM layer revealed a dynamic process of the domain wall motion during switching in contrast to the experimentally observed magnetic relaxed states. This difference could be explained by the additional local field arising from the FI layer, which is absent in the model. With this exception, the simulations replicated the two switching mechanisms of both systems.

High-resolution magnetic force microscopy together with micromagnetic modeling gave detailed insights into which magnetic system parameters are responsible for the complex magnetization reversal process of these ferri-/ferromagnetic exchange-coupled double-layer structures. These insights are crucial for the realization of submicron high energy density permanent magnets and spintronic devices. The implications are not only restricted to antiferromagnetically coupled ferri-/ferromagnetic bilayers but are also valid for further exchange-coupled composite media.[38,39] We thus conclude that this work will be beneficial for the understanding of the magnetization reversal of exchange-coupled structures that is potentially interesting for various applications.

AUTHOR INFORMATION

Corresponding Author

　Michael Heigl − *Institute of Physics, University of Augsburg, Augsburg 86159, Germany;* ⊙ orcid.org/0000-0001-6470-6457; Email: michael.heigl@physik.uni-augsburg.de

Authors

　Christoph Vogler − *Faculty of Physics, University of Vienna, Vienna 1090, Austria*

　Andrada-Oana Mandru − *Empa−Swiss Federal Laboratories for Materials Science and Technology, Dübendorf CH-8600, Switzerland*

　Xue Zhao − *Empa−Swiss Federal Laboratories for Materials Science and Technology, Dübendorf CH-8600, Switzerland*

　Hans Josef Hug − *Empa−Swiss Federal Laboratories for Materials Science and Technology, Dübendorf CH-8600, Switzerland; Department of Physics, University of Basel, Basel CH-4056, Switzerland;* ⊙ orcid.org/0000-0002-1281-4138

　Dieter Suess − *Christian Doppler Laboratory for Advanced Magnetic Sensing and Materials, Faculty of Physics, University of Vienna, Vienna 1090, Austria*

　Manfred Albrecht − *Institute of Physics, University of Augsburg, Augsburg 86159, Germany*

Complete contact information is available at:
https://pubs.acs.org/10.1021/acsanm.0c01835

Notes

The authors declare no competing financial interest.

ACKNOWLEDGMENTS

REFERENCES

(1) Fischbacher, J.; Kovacs, A.; Oezelt, H.; Gusenbauer, M.; Schrefl, T.; Exl, L.; Givord, D.; Dempsey, N. M.; Zimanyi, G.; Winklhofer, M.; Hrkac, G.; Chantrell, R.; Sakuma, N.; Yano, M.; Kato, A.; Shoji, T.; Manabe, A. On the limits of coercivity in permanent magnets. *Appl. Phys. Lett.* **2017**, *111*, No. 072404.

(2) Zeng, H. X.; Yu, H. Y.; Zhou, Q.; Zhang, J. S.; Liao, X. F.; Liu, Z. W. Clarifying the effects of La and Ce in the grain boundary diffusion sources on sintered NdFeB magnets. *Mater. Res. Express* **2019**, *6*, 106105.

(3) Kim, T.-H.; Sasaki, T. T.; Ohkubo, T.; Takada, Y.; Kato, A.; Kaneko, Y.; Hono, K. Microstructure and coercivity of grain boundary diffusion processed Dy-free and Dy-containing Nd-Fe-B sintered magnets. *Acta Mater.* **2019**, *172*, 139.

(4) Kneller, E. F.; Hawig, R. The exchange-spring magnet: a new material principle for permanent magnets. *IEEE Trans. Magn.* **1991**, *27*, 3588.

(5) Ungureanu, M.; Dumesnil, K.; Dufour, C.; Gonzalez, N.; Wilhelm, F.; Smekhova, A.; Rogalev, A. Using a zero-magnetization ferromagnet as the pinning layer in exchange-bias systems. *Phys. Rev. B* **2010**, *82*, 174421.

(6) Hauet, T.; Mangin, S.; Montaigne, F.; Borchers, J. A.; Henry, Y. Tuning exchange-bias properties by thermal effects in a hard/soft bilayer. *Appl. Phys. Lett.* **2007**, *91*, No. 022505.

(7) Patra, M.; Thakur, M.; Majumdar, S.; Giri, S. The exchange bias effect in phase separated Nd$_{1-x}$Sr$_x$CoO$_3$ at the spontaneous ferromagnetic/ferrimagnetic interface. *J. Phys.: Condens. Matter* **2009**, *21*, 236004.

(8) Romer, S.; Marioni, M. A.; Thorwarth, K.; Joshi, N. R.; Corticelli, C. E.; Hug, H. J.; Oezer, S.; Parlinska-Wojtan, M.; Rohrmann, H. Temperature dependence of large exchangebias in TbFe-Co/Pt. *Appl. Phys. Lett.* **2017**, *101*, 222404.

(9) Tokunaga, T.; Taguchi, M.; Fukami, T.; Nakaki, Y.; Tsutsumi, K. Study of interface wall energy in exchange-coupled double-layer film. *J. Appl. Phys.* **1990**, *67*, 4417.

(10) Hauet, T.; Montaigne, F.; Hehn, M.; Henry, Y.; Mangin, S. Magnetoresistance in an amorphous exchange-coupled bilayer. *Phys. Rev. B* **2009**, *79*, 224435.

(11) Watson, S. M.; Hauet, T.; Borchers, J. A.; Mangin, S.; Fullerton, E. E. Interfacial magnetic domain wall formation in perpendicular-anisotropy, exchange-spring films. *Appl. Phys. Lett.* **2008**, *92*, 202507.

(12) Mangin, S.; Montaigne, F.; Schuhl, A. Interface domain wall and exchange bias phenomena in ferrimagnetic/ferrimagnetic bilayers. *Phys. Rev. B* **2003**, *68*, 140404.

(13) Mangin, S.; Hauet, T.; Henry, Y.; Montaigne, F.; Fullerton, E. E. Influence of lateral domains and interface domain walls on exchange-bias phenomena in **GbFe/TdFe** bilayers. *Phys. Rev. B* **2006**, *74*, No. 024414.

(14) Mangin, S.; Hauet, T.; Fischer, P.; Kim, D. H.; Kortright, J. B.; Chesnel, K.; Arenholz, E.; Fullerton, E. E. Influence of interface exchange coupling in perpendicular anisotropy [Pt/Co]$_{50}$/TbFe bilayers. *Phys. Rev. B* **2008**, *78*, No. 024424.

(15) Lin, C.-C.; Lai, C.-H.; Jiang, R.-F.; Shieh, H.-P. D. High interfacial exchange energy in TbFeCo exchange-bias films. *J. Appl. Phys.* **2003**, *93*, 6832.

(16) Canet, F.; Mangin, S.; Bellouard, C.; Piecuch, M. Positive exchange bias in ferromagnetic-ferrimagnetic bilayers: FeSn/FeGd. *Europhys. Lett.* **2000**, *52*, 594.

(17) Hebler, B.; Böttger, S.; Nissen, D.; Abrudan, R.; Radu, F.; Albrecht, M. Influence of the Fe-Co ratio on the exchange coupling in TbFeCo/[Co/Pt] heterostructures. *Phys. Rev. B* **2016**, *93*, 184423.

(18) Dieny, B.; Speriosu, V. S.; Parkin, S. S. P.; Gurney, B. A.; Wilhoit, D. R.; Mauri, D. Giant magnetoresistive in soft ferromagnetic multilayers. *Phys. Rev. B* **1991**, *43*, 1297.

(19) Radu, F.; Abrudan, R.; Radu, I.; Schmitz, D.; Zabel, H. Perpendicular exchange bias in ferrimagnetic spin valves. *Nat. Commun.* **2012**, *3*, 715.

(20) Redon, O.; Freitas, P. P. Mechanism of exchange anisotropy and thermal stability of spin valves biased with ultrathin TbCo layers. *J. Appl. Phys.* **1998**, *83*, 2851.

(21) Lai, C.-H.; Wu, Z.-H.; Lin, C.-C.; Huang, P. H. Thermally assisted-writing giant magnetoresistance with perpendicular magnetization. *J. Appl. Phys.* **2005**, *97*, 10C511.

(22) Liao, J.; He, H.; Zhang, Z.; Ma, B.; Jin, Q. Y. Enhanced difference in switching fields for perpendicular magnetic spin valves with a composite [Co/Ni]$_N$/TbCo reference layer. *J. Appl. Phys.* **2011**, *109*, No. 023907.

(23) Lin, M.-S.; Lai, C.-H.; Liao, Y.-Y.; Wu, Z.-H.; Huang, S.-H.; Jiang, R.-F. Perpendicular giant magnetoresistance composed of [Co/Pt] multilayer and CoFe/TbCo. *J. Appl. Phys.* **2006**, *99*, No. 08T106.

(24) Bersweiler, M.; Lacour, D.; Dumesnil, K.; Montaigne, F.; Hehn, M. Phase diagram in exchange-coupled CoTb/[Co/Pt] multilayer-based magnetic tunnel junctions. *Phys. Rev. B: Condens. Matter Mater. Phys.* **2015**, *92*, 224431.

(25) Romer, S.; Marioni, M. A.; Thorwarth, K.; Joshi, N. R.; Corticelli, C. E.; Hug, H. J.; Oezer, S.; Parlinska-Wojtan, M.; Rohrmann, H. Temperature dependence of large exchange-bias in TbFe-Co/Pt. *Appl. Phys. Lett.* **2012**, *101*, 222404.

(26) Schubert, C.; Hebler, B.; Schletter, H.; Liebig, A.; Daniel, M.; Abrudan, R.; Radu, F.; Albrecht, M. Interfacial exchange coupling in Fe-Tb/[Co/Pt] heterostructures. *Phys. Rev. B* **2013**, *87*, No. 054415.

(27) Hebler, B.; Reinhardt, P.; Katona, G. L.; Hellwig, O.; Albrecht, M. Double exchange bias in ferrimagnetic heterostructures. *Phys. Rev. B* **2017**, *95*, 104410.

(28) Vas'kovskiy, V. O.; Svalov, A. V.; Balymov, K. G.; Kulesh, N. A. Effect of annealing on the magnetic anisotropy and hysteretic properties of film structures containing Tb-Co amorphous layers. *Phys. Met. Metallogr.* **2012**, *113*, 862.

(29) Vogler, C.; Heigl, M.; Mandru, A.-O.; Hebler, B.; Marioni, M.; Hug, H. J.; Albrecht, M.; Suess, D. Hysteresis-free magnetization reversal of exchange-coupled bilayers with finite magnetic anisotropy. *Phys. Rev. B* **2020**, *102*, No. 014429.

(30) Zhao, X.; Mandru, A.-O.; Vogler, C.; Marioni, M. A.; Suess, D.; Hug, H. J. Magnetization Reversal of Strongly Exchange-Coupled Double Nanolayers for Spintronic Devices. *ACS Appl. Nano Mater.* **2019**, *2*, 7478.

(31) Heigl, M.; Wendler, R.; Haugg, S. D.; Albrecht, M. Magnetic properties of Co/Ni-based multilayers with Pd and Pt insertion layers. *J. Appl. Phys.* **2020**, *127*, 233902.

(32) Hug, H. J.; Stiefel, B.; van Schendel, P. J. A.; Moser, A.; Martin, S.; Güntherodt, H.-J. A low temperature ultrahigh vaccum scanning force microscope. *Rev. Sci. Instrum.* **1999**, *70*, 3625.

(33) Zhao, X.; Schwenk, J.; Mandru, A. O.; Penedo, M.; Bacani, M.; Marioni, M. A.; Hug, H. J. Magnetic force microscopy with frequency-modulated capacitive tip−sample distance control. *New J.Phys.* **2018**, *20*, No. 013018.

(34) Makarov, D.; Lee, J.; Brombacher, C.; Schubert, C.; Fuger, M.; Suess, D.; Fidler, J.; Albrecht, M. Perpendicular FePt-based exchange-coupled composite media. *Appl. Phys. Lett.* **2010**, *96*, No. 062501.

(35) Hebler, B.; Hassdenteufel, A.; Reinhardt, P.; Karl, H.; Albrecht, M. Ferrimagnetic Tb−Fe Alloy Thin Films: Composition and Thickness Dependence of Magnetic Properties and All-Optical Switching. *Front. Mater.* **2016**, *3*, 8.

(36) Graves, C. E.; Reid, A. H.; Wang, T.; Wu, B.; de Jong, S.; Vahaplar, K.; Radu, I.; Bernstein, D. P.; Messerschmidt, M.; Müller, L.; Coffee, R.; Bionta, M.; Epp, S. W.; Hartmann, R.; Kimmel, N.; Hauser, G.; Hartmann, A.; Holl, P.; Gorke, H.; Mentink, J. H.; Tsukamoto, A.; Fognini, A.; Turner, J. J.; Schlotter, W. F.; Rolles, D.; Soltau, H.; Strüder, L.; Acremann, Y.; Kimel, A. V.; Kirilyuk, A.; Rasing, T.; Stöhr, J.; Scherz, A. O.; Dürr, H. A. Nanoscale spin reversal by non-local angular momentum transfer following ultrafast laser excitation in ferrimagnetic GdFeCo. *Nat. Mater.* **2013**, *12*, 293.

(37) Abert, C.; Exl, L.; Bruckner, F.; Drews, A.; Suess, D. magnum.fe: A micromagnetic finite-element simulation code based on FEniCS. *J. Magn. Magn. Mater.* **2013**, *345*, 29.

(38) Victora, R. H.; Shen, X. Exchange Coupled Composite Media. *Proc. IEEE* **2008**, *96*, 1799.

(39) Suess, D.; Schrefl, T.; Fähler, S.; Kirschner, M.; Hrkac, G.; Dorfbauer, F.; Fidler, J. Exchange spring media for perpendicular recording. *Appl. Phys. Lett.* **2005**, *87*, No. 012504.